Electronic Supplementary Information

for

Enhanced Performance of Dye-Sensitized Solar Cells based on TiO_2 Nanotube Membranes using Optimized Annealing Profile

by Fatemeh Mohammadpour,[1] Mahmood Moradi,[1] Kiyoung Lee,[2] Gihoon Cha,[2] Seulgi So,[2] Axel Kahnt,[3] Dirk Michael Guldi,[3] Marco Altomare[2] and Patrik Schmuki[2,4,*]

[1] Department of Physics, Faculty of Science, University of Shiraz, Shiraz 71454, Iran

[2] Department of Material Science and Engineering, WW4-LKO, University of Erlangen-Nuremberg, Martensstrasse 7, D-91058 Erlangen, Germany

[3] Department of Chemistry and Pharmacy and Interdisciplinary Center for Molecular Materials, University of Erlangen-Nuremberg, Egerlandstrasse 3, D-91058 Erlangen, Germany

[4] Department of Chemistry, King Abdulaziz University, Jeddah, Saudi Arabia

Contents

- Scheme S1 - Cell configurations pp. 1
- Anodic growth of TiO_2 nanotube layers and membrane fabrication pp. 2
- Fabrication of photo-anodes and DSSCs pp. 3
- Characterization of photo-anodes and DSSCs pp. 4
- Figure S1 - XRD patterns of TiO_2 nanotube membrane-based photo-anodes pp. 6
- Figure S2 - J-V curves and photovoltaic characteristics pp. 7
- Figure S3 - J-V curve and IPCE spectra of a DSSC (masking conditions) pp. 8
- Figure S4 - IMPS measurements of bare photo-anodes pp. 9
- SEM and TEM characterization of TiO_2 nanotube membranes pp. 10
- Figure S5 - XPS analysis pp. 11
- Figure S6 - EDAX analysis pp. 12
- Table S1 - Crystallite mean size pp. 13
- Figure S7 - Results of (fs) pump-probe laser spectroscopy pp. 14
- References pp. 15

Scheme S1 - Sketch of a) back- and c), d) front-side illuminated TiO_2-based dye-sensitized solar cells. In the case of front-side illuminated DSSCs, the TiO_2 nanotube membrane can be transferred onto TiO_2 NP-coated FTO slides either in b) tube-top-up or c) tube-top-down configuration.

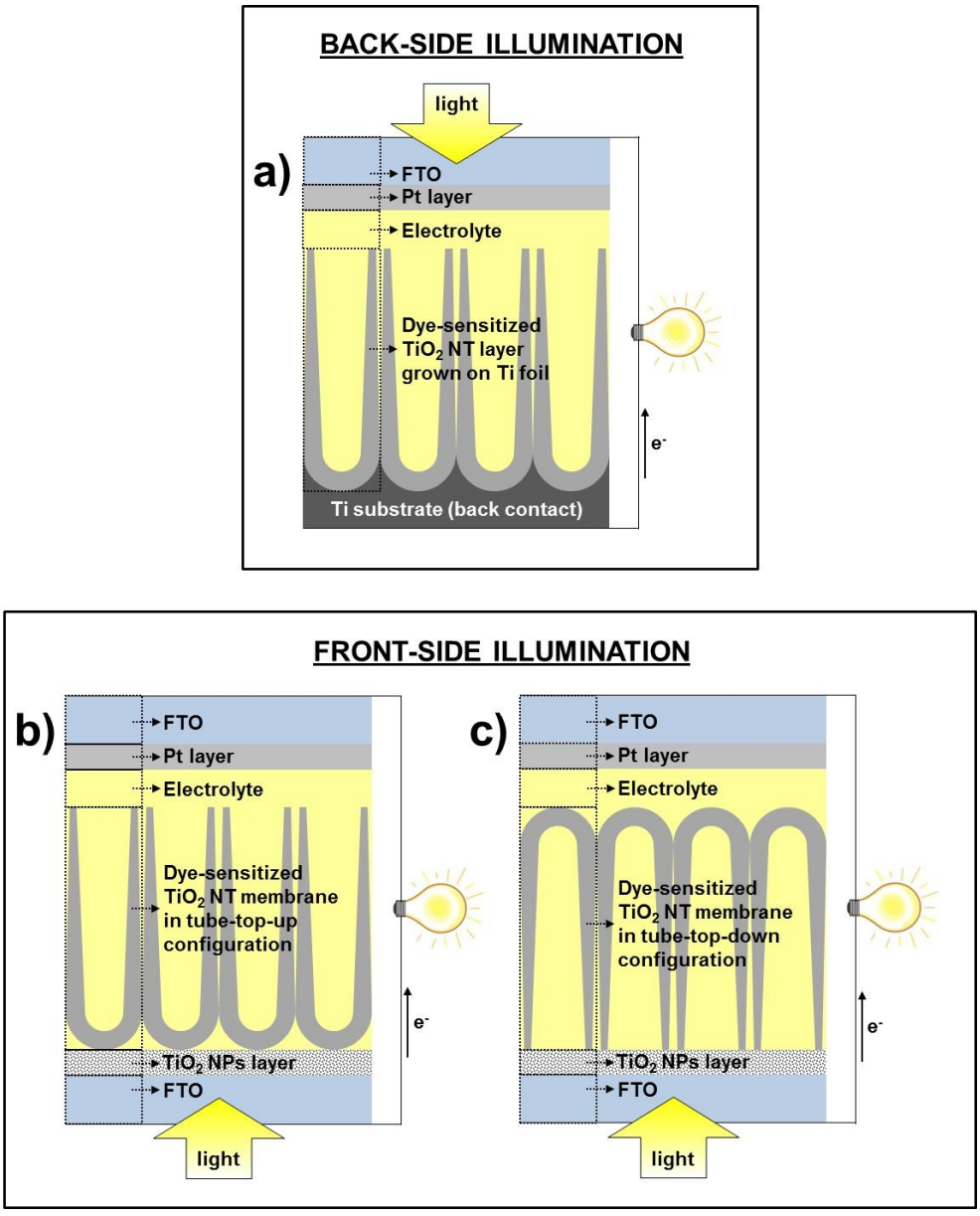

Anodic growth of TiO_2 nanotube layers and membrane fabrication

Highly ordered TiO_2 nanotube arrays were prepared by anodization of Ti foil (0.125 mm thickness, 99.7 % purity, Advent) in a two electrode electrochemical cell by using a Pt sheet as counter electrode. Prior to anodization, the Ti foils were cleaned by sonication in acetone and ethanol (10 min each) followed by rinsing in de-ionized water (DI) and drying in a N_2 stream.

The anodization experiments were performed at 60 V at room temperature in an electrolyte composed of ethylene glycol with 0.15 M NH_4F and 3 vol.% deionized (DI) water. TiO_2 nanotube layers with a thickness of *ca*. 20 μm were produced by anodizing the Ti substrates in the above mentioned conditions for 1 h.

For producing TiO_2 nanotube membranes we followed a re-anodization approach introduced by Chen *et al.* [1]. For this, the as-prepared TiO_2 nanotube layers were annealed in air at 350 °C for 1 h. Then, the crystallized TiO_2 nanotube samples were anodized a second time in the same experimental conditions of the first anodization step. Afterwards, the nanotube layers were detached from the Ti substrate by immersing the tube layers in an aqueous 0.07 M HF solution at 30 °C: the tube layers formed by the second anodization step were still amorphous and therefore underwent preferential chemical dissolution in the HF solution so that the tube layers formed by the first anodization step and pre-annealed could be lifted off as free-standing membranes.

Fabrication of the photo-anodes and DSSCs

The photo-anodes were prepared after detachment of the TiO_2 nanotube layers by transferring the 20 μm-thick membranes onto FTO slides (7 Ω m^{-2}) that were previously coated by doctor-blade technique with a 2 μm-thick film of a commercial TiO_2 nanoparticle paste (Ti-Nanoxide HT, Solaronix). The TiO_2 nanoparticle layer granted good adhesion, mechanical stability and established good electric contact between tubes and FTO. The membranes were transferred onto FTO either in tube-top-up or tube-top-down (*i.e.*, up-side down) configurations (see scheme S1). A "reference cell" was also fabricated by using a 20 μm-thick TiO_2 nanoparticle layer as photo-anode (deposited by doctor-blade technique) instead of the detached nanotube membranes. After drying in air for about 20 min, all the photo-anodes were annealed in air at different temperatures (range of 350-650 °C) for 1 h, with a heating/cooling rate of 10, 30 and 60 °C min^{-1} by using a Rapid Thermal Annealer (Jipelec JetFirst100). Precisely, when screening the different annealing temperatures, a slow heating profile, *i.e.*, 10 °C min^{-1}, was always used. On the other hand, when screening the effect of different heating rates (10, 30 and 60 °C min^{-1}), all the photo-anodes were annealed at 500 °C.

For fabricating the dye-sensitized cells, the crystalline photo-anodes were firstly immersed into a 300 μM dye solution (D719, Everlight, Taiwan) at 40 °C for 24 h. After dye-sensitization the samples were rinsed with acetonitrile to remove the non-chemisorbed dye and then were dried in a N_2 stream. The fabrication of the DSSCs was completed by sandwiching the crystalline dye-sensitized photo-anodes with Pt coated FTO glass as counter electrode using a hot-melt spacer (25μm, Surlyn, Dupont). Finally, the electrolyte (Io-li-tec, ES-0004) was introduced within the interspace of the DSSCs.

Characterization of the photo-anodes and DSSCs

For morphological characterization of the TiO_2-based photo-anodes, a field-emission scanning electron microscope (FE-SEM, Hitachi SEM FE 4800) and transmission electron microscopy (Philips CM 30 T/STEM microscope) were used.

For determining the crystallographic features of the photo-anodes, X-ray diffraction analysis (XRD) was performed with an X'pert Philips MPD equipped with a Panalytical X´celerator detector using graphite monochromized Cu Kα radiation (λ = 1.54056 Å).

The chemical composition of the TiO_2 scaffolds was determined by energy dispersive X-ray analysis (EDAX Genesis) fitted to the Hitachi FE-SEM S4800, and by X-ray photoelectron spectroscopy (XPS, PHI 5600, US).

The current-voltage characteristics of the different DSSCs were measured under simulated AM 1.5 front-side illumination provided by a solar simulator (300 W Xe with optical filter, Solarlight) and by applying an external bias (from - 50 mV up to + 900 mV) to the cell and measuring the generated photocurrent with a Keithley model 2420 digital source meter. Step size and holding time were 23.75 mV and 100 ms, respectively. The active area was defined by the 0.2 cm^2-sized opening of the Surlyn seal and a scattering background was used.

Dye loading on the photo-anodes was measured by immersing the different dye-sensitized TiO_2 scaffolds in 5 mL of a 10 mM NaOH aqueous solution for 30 minutes. Then the optical absorption of the solutions was measured by a UV-Vis Spectrophotometer (Lambda XLS+, Perkin Elmer).

Intensity modulated photocurrent spectroscopy (IMPS) measurements of the different dye-sensitized TiO_2 photo-anodes were carried out in aqueous 0.1 M Na_2SO_4 solutions by using modulated light (10 % modulation depth) from a high power green LED (λ = 530 nm). The modulation frequency was controlled by a frequency response analyzer (FRA, Zahner). The light intensity incident on the cell was measured using a calibrated Si photodiode. A three electrode electrochemical cell was used, with a Pt foil as counter electrode and an Ag/AgCl reference electrode.

Incident photon-to-current conversion efficiency (IPCE) measurements were performed with a 150 W Xe arc lamp (LOT-Oriel Instruments) with an Oriel Cornerstone 7400 1/8 m monochromator. The light intensity was measured with an optical power meter.

To study the charge transport process upon photo-excitation of the different TiO_2 photo-anodes, transient absorption spectroscopy based on femtosecond (fs) pump-probe experiments were carried out. The 20 μm-thick photo-anodes that were actually used for fabricating the DSSCs could not be employed for these measurements as too thick for transmitting the light pulse, that is, the pulse irradiated on the samples was fully absorbed and no transmitted signal could be measured. Therefore, the pump-probe experiments were performed on *ca*. 3 μm-thick TiO_2 nanotube layer grown on quartz slides and crystallized in air at 500 °C with heating rate of 10, 30 and 60 °C min^{-1}. Quartz slides as substrates for the

tube layers were preferred over FTO glasses since the used excitation wavelength was in the UV range (see below). The tube layers were grown by fully anodizing the 1 μm-thick Ti layers that were evaporated on the quartz substrates. The anodization experiments were performed in the same electrolyte and at the same potential used for fabricating the membranes, and led to TiO_2 nanotubes showing comparable features in terms of morphology and phase composition upon crystallization. The pump-probe measurements were performed with a CPA-2110 femtosecond laser (Clark MXR, output 775 nm, 1 kHz, and 150 fs pulse width) using a transient absorption detection system (TAPPS Helios, Ultrafast Systems). The excitation wavelength was generated by third harmonic generation (258 nm) and was characterized by a pulse width of < 150 fs and energy of 200 nJ per pulse.

The obtained transient absorption spectra (reported in Fig. 3(a)-(d) in the main text) are well in line with those typically measured for TiO_2 [2-6]. According to the literature, the transient absorption in the visible region (between 400 and 600 nm, this depending on the structural features of the material) is mainly assigned to the holes formed upon photo-excitation. This signal is overlaid by the strong absorption of the trapped electrons that is usually observed in the region between 500 and 900 nm. Furthermore, the transient absorption of the "free" electrons is observed over the entire optical spectrum, although showing particularly strong absorptions in the near infrared (NIR) region. Besides, we also observed the transient absorption/stimulated emission of/from electron-hole recombination induced by the probe light.

The transients that were observed for each sample are represented by the sum of the absorption of the three independent species (holes, trapped and "free" electrons). Therefore, the decay curves of the transients were fitted to three exponential functions (at 550, 800 and 1250 nm). Since all three transient species show overlapping absorptions, global fits were performed in which the three lifetimes are global variables and the non-decaying components were treated as "offset" (a summary of the data is reported in Fig. 3(e) in the main text).

Figure S1 - a) XRD patterns of TiO_2 nanotube membranes that were transferred onto TiO_2 NP-coated FTO slides in tube-top-down configuration and annealed at 500 °C by using different heating rates (10, 30 and 60 °C min-1). XRD patterns of TiO_2 nanotube membranes that were transferred onto TiO_2 NP-coated FTO slides in b) tube-top-up and c) tube-top-down configurations (see scheme S1(b) and (c)) and annealed in air, at different temperatures (350-650 °C range) for 1 h, with a heating/cooling rate of 10 °C min^{-1}.

The XRD patterns measured for these photo-anodes show all the tube membranes to be composed of 100 % anatase phase, this regardless of photo-anode configuration and annealing temperature.

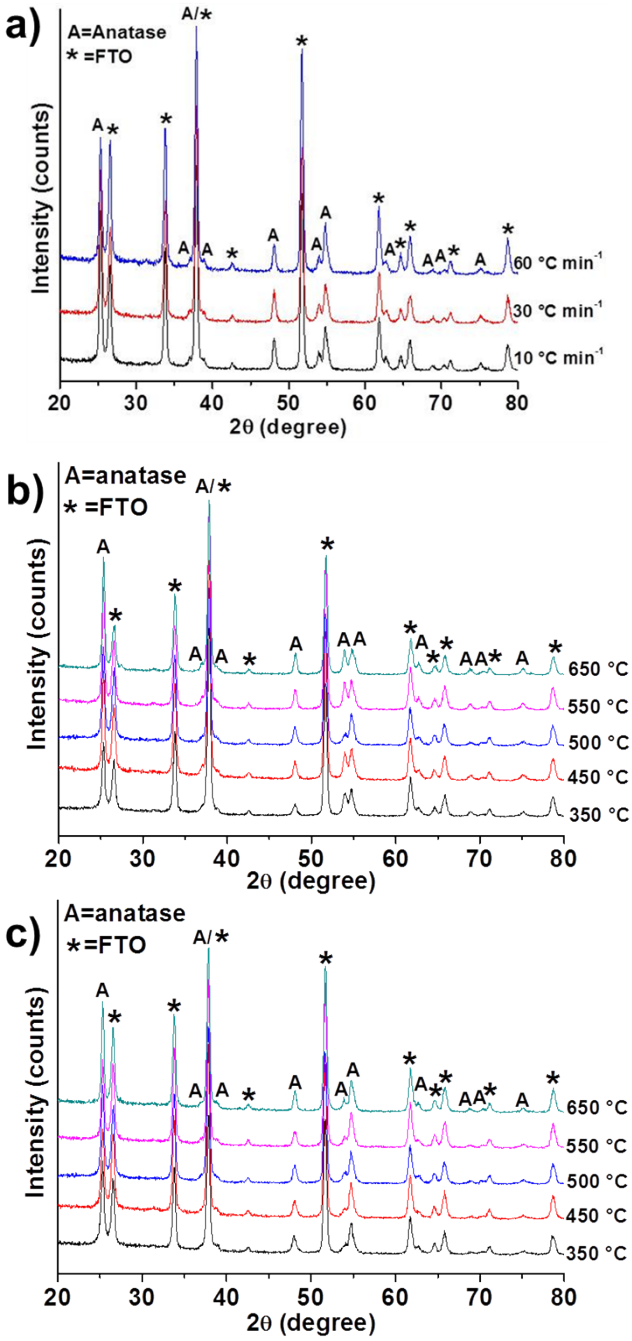

Figure S2 - a), b) J-V curves and c), d) photovoltaic characteristics of TiO_2 nanotube membrane-based DSSCs measured under simulated AM 1.5 illumination. To fabricate the photo-anodes, the TiO_2 nanotube membranes were transferred onto TiO_2 NP-coated FTO slides in a), c) tube-top-up and b), d) tube-top-down configurations. The photo-anodes were crystallized by annealing in air, at different temperatures (350-650 °C range) for 1 h, with a heating/cooling rate of 10 °C min^{-1}. Insets in a) and b) represent a sketch of tube-top-up and tube-top-down configurations, respectively.

These experiments show that the tube-top-down configuration of the photo-anode along with the annealing temperature of 500°C represent the experimental conditions leading to dye-sensitized solar cells with enhanced efficiencies (*e.g.*, up to 8.19 %). These results are well in line with the literature [7,8], and can be explained by considering that *(i)* a tube-top-down configuration of the tube membranes leads to a larger dye-loading (better access of the dye to the TiO_2 nanoparticle layer beneath the tubes); and *(ii)* the annealing at 500°C represents an optimized thermal treatment in view of obtaining optimized crystallographic properties of the tubes.

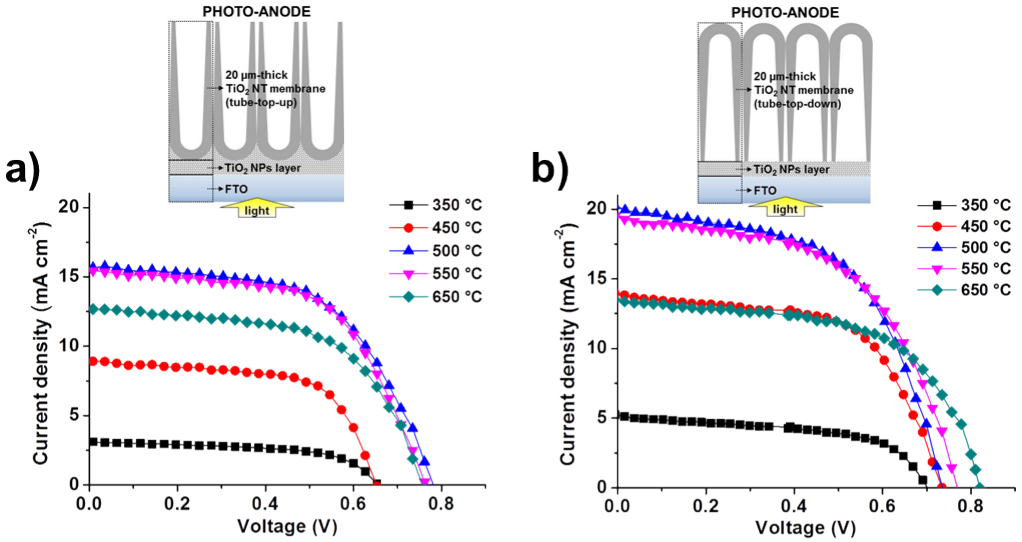

c)

T (°C)	Dye-loading (nM cm^{-2})	J_{sc} (mA cm^{-2})	V_{oc} (V)	FF (%)	η (%)
350	78	3.12	0.66	58	1.19
450	86	8.94	0.65	64	3.71
500	87	15.75	0.78	57	7.00
550	66	15.50	0.76	59	6.95
650	44	12.71	0.76	59	5.67

d)

T (°C)	Dye-loading (nM cm^{-2})	J_{sc} (mA cm^{-2})	V_{oc} (V)	FF (%)	η (%)
350	92	5.19	0.70	55	2.00
450	100	13.93	0.74	59	6.09
500	115	20.19	0.73	56	8.19
550	74	19.44	0.77	54	8.10
650	60	13.52	0.82	59	6.49

Figure S3 - a) J-V curve measured under simulated AM 1.5 illumination and b) example of IPCE spectrum (black curve) and relative integrated current density (red curve) of TiO_2 nanotube membrane-based DSSC. Both (a) and (b) were measured under full shadow masking conditions, and in absence of scattering background. To fabricate the photo-anode, the TiO_2 nanotube membrane was transferred onto a TiO_2 NP-coated FTO slide in tube-top-down configurations. The photo-anode was crystallized by annealing in air, at 500°C for 1 h, with a heating/cooling rate of 30°C min^{-1}.

These results show that a decrease of J_{sc} was observed to a value of *ca*. 17.3 mA cm^{-2} (well in line with the theoretical limit), while the FF was improved. This overall resulted only in a slight decrease of the cell efficiency to η=8.6%.

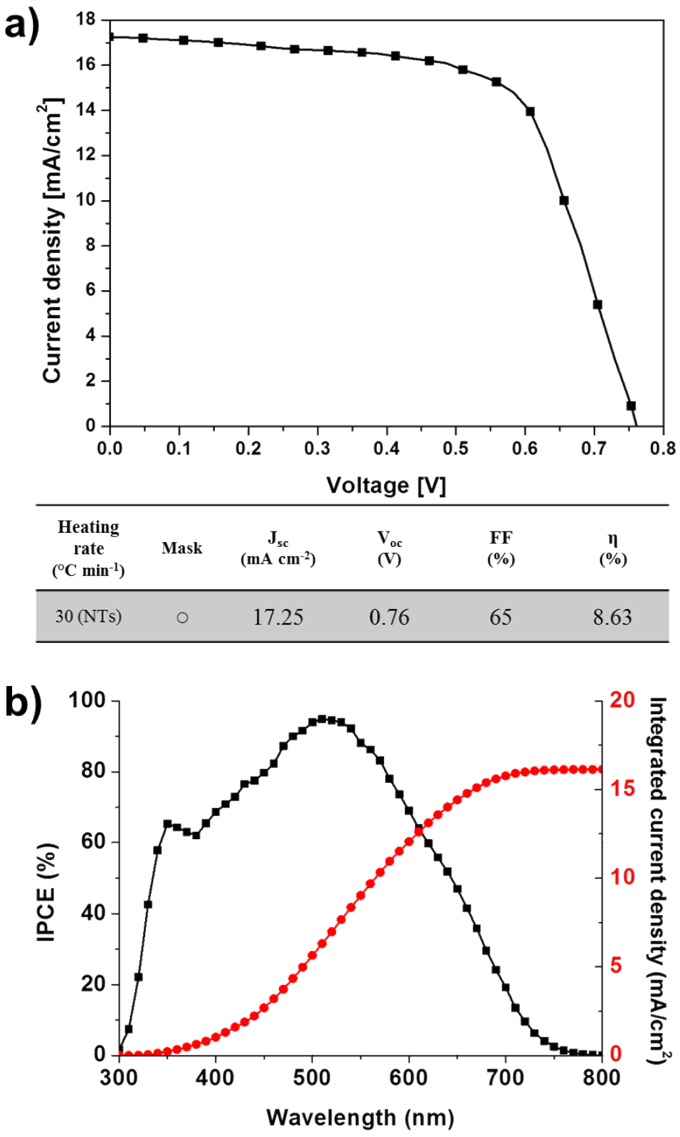

Heating rate (°C min^{-1})	Mask	J_{sc} (mA cm^{-2})	V_{oc} (V)	FF (%)	η (%)
30 (NTs)	○	17.25	0.76	65	8.63

Figure S4 - Intensity modulated photocurrent spectroscopy (IMPS) measurements were carried out in aqueous 0.1 M Na_2SO_4 solutions on bare (*i.e.*, without dye-sensitization) TiO_2 nanotube membrane-based photo-anodes annealed in air at 500 °C with heating rates of 10 and 30 °C min^{-1}. A three electrode electrochemical cell was used, with a Pt foil as counter electrode and an Ag/AgCl reference electrode. The experiments were performed by using modulated light (10 % modulation depth) from a high power LED (λ = 365 nm). The modulation frequency was controlled by a frequency response analyzer (FRA, Zahner). The light intensity incident on the cell was measured using a calibrated Si photodiode. The photocurrent of the cell was measured using a Zahner electrochemical interface that fed back into the FRA for analysis.

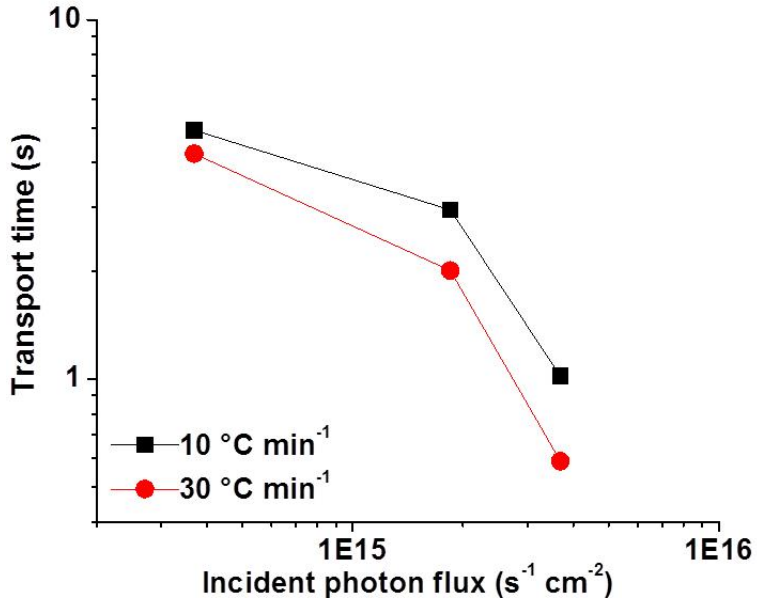

SEM and TEM characterization of the TiO_2 tube membranes

From the top-view SEM pictures (shown in the main text - Fig 2(a), (c) and (e) - and taken by cracking the anodic film at a middle height along the tube length) it can be seen that all the tubes show an outer diameter of *ca*. 140-160 nm regardless of the annealing conditions. Nevertheless, a heating rate of 10 $^{\circ}C$ min^{-1} leads to a clear separation of the inner and outer shells of the nanotubes (Fig. 2(a)) [9-11]. This separation could not be observed when tubes were subjected to a more rapid ramping in the annealing process (shown in Fig. 2(c),(e)). In particular, we found that a more rapid annealing led to a merging of the two shells so that an apparently "single-walled" tubular structure was obtained upon crystallization.

Further significant morphological features could be observed by TEM investigations (see Fig 2(b), (d) and (f) in the main text). First, a slow annealing leads to nanotubes with corrugated structure of the walls. This is most likely ascribed to the presence of the inner shell of tube which in this case exhibits a "nanoporous" texture (see Fig. 2(b)) [11]. Second, for these tubes the grain boundaries are clearly visible as fractures along the tube walls (highlighted in Fig. 2(b)). Conversely, the rapidly annealed tubes show a more robust morphology and do not exhibit sharp discontinuities along the tube walls (Fig. 2(d),(f)). Moreover, differences in the tube wall thickness can be seen when comparing tubes crystallized by using different heating rates. The nanotubes crystallized with heating rate of 60 $^{\circ}C$ min^{-1} were *ca*. 28 nm thick while those annealed at 30 $^{\circ}C$ min^{-1} were 35 nm thick. In line with this trend, we observed that the tubes annealed by using a rate of 10 $^{\circ}C$ min^{-1} showed about 46 nm-thick walls, with outer and inner shells of 27 and 19 nm in thickness, respectively.

Besides the effects on the morphology, we also found that the annealing conditions slightly affected both the crystallinity and the chemical composition of the tubes. In fact, as shown by the SAED patterns reported in Fig. 2, the typical reflections of TiO_2 anatase phase become brighter (*i.e.*, more intense) when increasing the rate of annealing, meaning that the rapid annealing led to nanotubes with a higher degree of crystallinity. In spite of this, no relevant change of crystallite mean size could be observed for the different annealing conditions (see data in Table S1).

On the other hand, for the chemical composition determined by XPS and EDAX analysis of the different photo-anodes, we found a clearly lower carbon and fluorine contents for rapidly annealed tubes (see Fig. S5 and S6). This may explain the material loss that leads to thinner tube walls, that is, a fast heating rate induces a larger release of carbonaceous species from the inner shell of the tubes (carbon is up-taken in the inner tube shell from the organic-based electrolyte during anodization [10,11]).

Figure S5 - XPS analysis of TiO_2 nanotube membrane-based photo-anodes annealed in air at 500 °C with heating rates of 10 and 30 °C min^{-1}: a) XPS survey; b) high-resolution spectra of the C 1s area; c) summary of the XPS data.

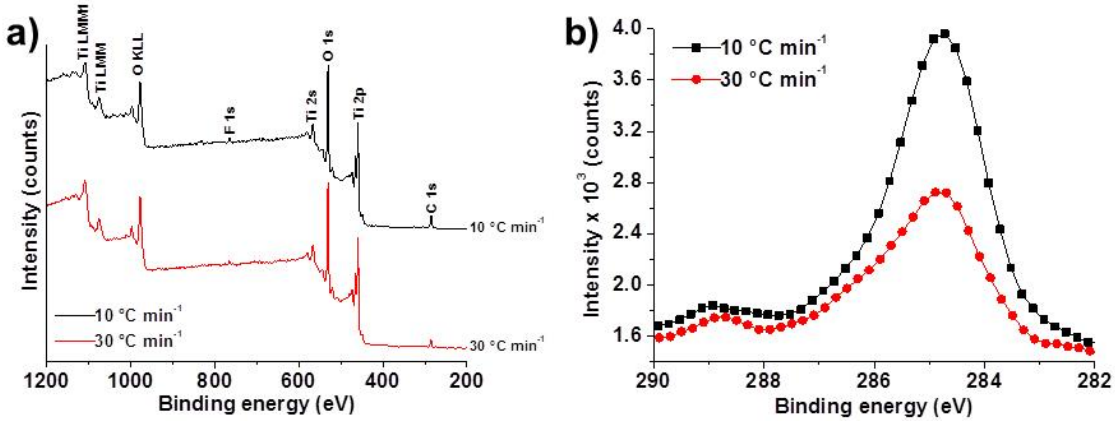

c)

Summary of XPS data

Heating rate (°C min^{-1})	Element	Wt. %	At. %
10	C 1s	9.15	17.73
	O 1s	38.78	56.43
	F 1s	0.70	0.85
	Ti 2p	51.38	24.99
30	C 1s	5.46	11.05
	O 1s	40.30	61.18
	F 1s	0.31	0.40
	Ti 2p	53.93	27.37

Figure S6 - EDAX analysis of TiO_2 nanotube membrane-based photo-anodes annealed in air at 500 °C with heating rates of 10 and 30 °C min^{-1}: a) and b) EDAX spectra of the photo-anodes annealed with a heating rate of 10 and 30 °C min^{-1}, respectively; c) summary of the EDAX data.

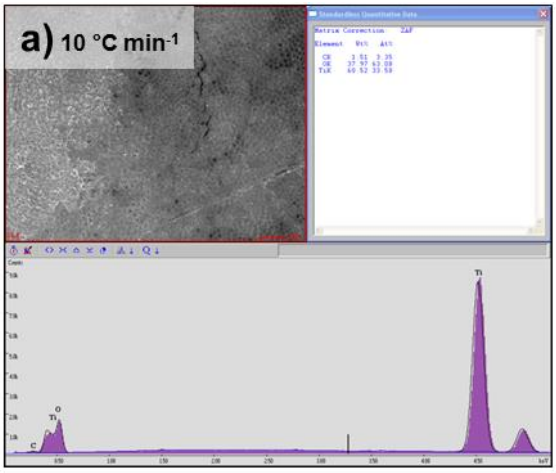

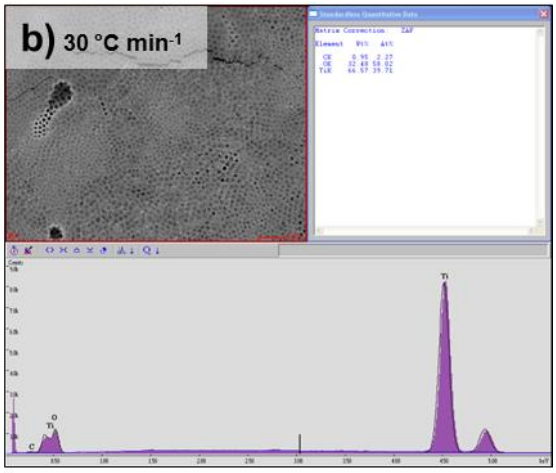

c)

Summary of EDAX data

Heating rate (°C min^{-1})	Element	Wt. %	At. %
10	C k	1.51	3.35
	O k	37.97	63.08
	Ti k	60.52	33.58
30	C k	0.95	2.27
	O k	32.48	58.02
	Ti k	66.57	39.71

Table S1 - Mean crystallite size for TiO_2 nanotubes annealed in air at 500 °C with heating rates of 10, 30 and 60 °C min^{-1}. The crystallite size was determined by: *i)* processing the XRD data by using the Sherrer equation applied to the main reflection of TiO_2 anatase phase ($2\theta = 25.3°$ corresponding to the (101) crystallographic face); *ii)* TEM investigation (each value represents the average of the size of ten different crystallites).

Average TiO_2 grain size for nanotubes annealed by different heating rates

Heating rate (°C min^{-1})	**from XRD data**	**from TEM analysis**
10	35.6	34.0
30	35.9	35.0
60	34.2	-

Figure S7 - a) Differential absorption spectra (visible and near-infrared) measured by femtosecond flash photolysis (258 nm) at different time delays of 1 ps (black), 10 ps (red), 100 ps (green), 1000 ps (blue), and 6500 ps (cyan); b) Relative absorption time profiles of the spectra a) at 550 nm (black), 800 nm (red) and 1200 nm (blue) corresponding to absorption of holes, trapped-electrons and free electron, respectively. Data in a) and b) were measured for *ca.* 3 µm-thick TiO_2 nanotube layers (grown on quartz slides) that were annealed at 500 °C with heating rate of 60 °C min^{-1}; c) data obtained by fitting the decay transient curves to three exponential functions (at 550, 800 and 1250 nm) in order to distinguish the contributions of the different transient species (*i.e.*, holes, trapped-electrons and free electron).

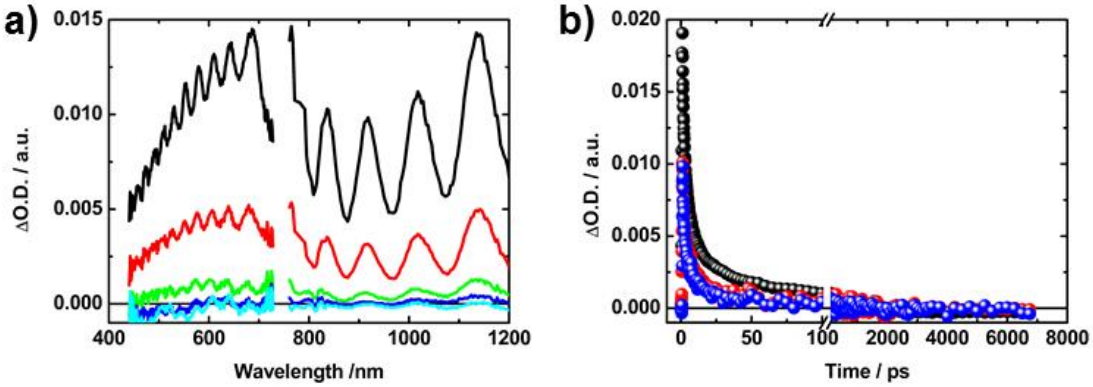

c)

Heating ramp (°C min^{-1})	λ (nm)	a_1	τ_1 (ps)	a_2	τ_2 (ps)	a_3	τ_3 (ps)	I_0
	550	0.45		0.48		0.07		$-2.33E^{-4}$
60	800	0.48	5.0	0.47	30.0	0.05	1339	$-7.95E^{-5}$
	1200	0.17		0.74		0.09		$1.901E^{-4}$

References

[1] Q. Chen, D. Xu, Large-Scale, Noncurling, and Free-Standing Crystallized TiO_2 Nanotube Arrays for Dye-Sensitized Solar Cells, *J. Phys. Chem. C* 2009, **113**, 6310-6314.

[2] A. Kahnt, C. Oelsner, F. Werner, D.M. Guldi, S.P. Albu, R. Kirchgeorg, K. Lee, P. Schmuki, Excited state properties of anodic TiO_2 nanotubes, *Appl. Phys. Lett.* 2013, **102**, 233109-1 - 233109-5.

[3] A. Hagfeldt, M. Grätzel, Light-Induced Redox Reactions in Nanocrystalline Systems, *Chem. Rev.* 1995, **95**, 49-68.

[4] X. Yang, N. Tamai, How Fast is Interfacial Hole Transfer? In Situ Monitoring of Carrier Dynamics in Anatase TiO_2 Nanoparticles by Femtosecond Laser Spectroscopy, *Phys. Chem. Chem. Phys*. 2001, **3**, 3393-3398.

[5] T. Yoshihara, R. Katoh, A. Furube, Y. Tamaki, M. Murai, K. Hara, S. Murata, H. Arakawa, M. Tachiya, Identification of Reactive Species in Photoexcited Nanocrystalline TiO_2 Films by Wide-Wavelength-Range (400-2500 nm) Transient Absorption Spectroscopy, *J. Phys. Chem. B* 2004, **108**, 3817-3823.

[6] Y. Tamaki, A. Furube, M. Murai, K. Hara, R. Katoh, M. Tachiya, Dynamics of Efficient Electron-Hole Separation in TiO_2 Nanoparticles Revealed by Femtosecond Transient Absorption Spectroscopy Under the Weak-Excitation Condition, *Phys. Chem. Chem. Phys*. 2007, **9**, 1453-1460.

[7] M. Dubey, M. Shrestha, Y. Zhong, D. Galipeau, H. He, TiO_2 nanotube membranes on transparent conducting glass for high efficiency dye-sensitized solar cells, *Nanotechnol*. 2011, **22**, 285201-1 – 285201-9.

[8] A. Ghicov, S.P. Albu, R. Hahn, D. Kim, T. Stergiopoulos, J. Kunze, C.-A. Schiller, P. Falaras, P. Schmuki, TiO_2 Nanotubes in Dye-Sensitized Solar Cells: Critical Factors for the Conversion Efficiency, *Chem. Asian J.* 2009, **4**, 520-525.

[9] S.P. Albu, A Ghicov, S. Aldabergenova, P. Drechsel, D. LeClere, G.E. Thompson, J.M. Macák, P. Schmuki, Formation of Double-Walled Nanotubes and Robust Anatase Membranes, *Adv. Mater*. 2008, **20**, 4135-4139.

[10] H. Mirabolghasemi, N. Liu, K. Lee, P. Schmuki, Formation of 'single walled' TiO_2 nanotubes with significantly enhanced electronic properties for higher efficiency dye-sensitized solar cells, *Chem. Commun.* 2013, **49**, 2067-2069.

[11] N. Liu, H. Mirabolghasemi, K. Lee, S.P. Albu, A. Tighineanu, M. Altomare, P. Schmuki, Anodic TiO_2 nanotubes: double walled *vs.* single walled, *Faraday Discuss*. 2013, **164**, 107-116.